LIMNOLOGY
and
OCEANOGRAPHY

ASLO

Limnol. Oceanogr. 63, 2018, 951–967

doi: 10.1002/lno.10682

Potential of marshes to attenuate storm surge water level in the Chesapeake Bay

Emma M. Glass, Juan L. Garzon ,* Seth Lawler, Eleonore Paquier, Celso M. Ferreira
Department of Civil, Environmental and Infrastructure Engineering, George Mason University, Fairfax, Virginia

Abstract

Storm surges from tropical and extratropical storms frequently impact coastal communities globally. While the potential of natural and nature-based features for coastal defenses has gained increased attention as a viable option for coastal flood protection, the lack of in situ measurements of storm surge attenuation has delayed their widespread utilization. We present the findings of a 3-yr water level monitoring campaign that resulted in a large collection (52 flood events) of attenuation rates from marsh transects located in two natural preserves in the U.S. mid-Atlantic region. Results show that the overall marsh attenuated water levels, exhibiting values up to 0.02 cm/m at Eastern Shore of Virginia National Wildlife Refuge (ES) and 0.03 cm/m at Magothy Bay Natural Preserve (MGB). In general, the greatest attenuation rates were observed at the marsh edge section. The reach close to the coastline revealed an amplification of the water level followed by water level attenuation toward the backside of the marsh. However, analyses of five major storms at ES demonstrated that, within each event, the ability of the upper marsh to attenuate water level decreased with higher inundation heights. Additionally, small spatial scales of the marsh platform, geomorphological features such as channels, elevated surrounding forests and levees seem to play a major role in reducing the attenuation rates provided by the marshes. These results indicate that, while this type of marshland would provide storm surge attenuation during low inundation heights, these ecosystems would be less effective attenuating higher water depths from extreme events.

Severe tropical and extratropical storms have demonstrated their adverse effects on coastal communities around the globe, causing millions of dollars in damages annually, with the potential to cause even greater damage in the future (Wobus et al. 2013). Recently, the United States (U.S.) experienced the effects of Hurricanes Katrina (2005), Ike (2008), Irene (2011), Sandy (2012), and Matthew (2016) in some of the most well developed areas of the country. Damages from Hurricane Sandy and Hurricane Katrina alone totaled over 173 billion dollars, and led to nearly 2000 casualties (Cui and Caracoglia 2016). In addition to traditional "hard" structures such as levees and dikes designed to mitigate the impacts of coastal flood events, there is an increasing interest in the adoption of natural and nature-based features to support coastal resilience plans (Arkema et al. 2013; Sutton-Grier et al. 2015). Coastal wetlands, although most well known for being highly productive ecological environments (Lavoie et al. 2016), have also been found to be good candidates for natural protection of coastal communities against flooding (Arkema et al. 2013; Barbier et al. 2013). Additionally, by combining natural wetlands with man-made structures, the resilience of coastal communities to large storms could be significantly increased (Sutton-Grier et al. 2015). In the U.S., the Executive Office of the President of the United States' National Science and Technology Council (Committee on Environment and Resources National Science and Technology Council 2015) encouraged the transition toward installing greener infrastructure as a natural flood defense mechanism. While the potential coastal protection services of green infrastructure have been widely explored (Arkema et al. 2013; Sutton-Grier et al. 2015; Narayan et al. 2016), additional quantification of actual coastal protection mechanisms are necessary to effectively design nature-based coastal features for flood protection (National Research Council 2014).

Various studies have investigated coastal storm hydrodynamics and flood reduction in coastal wetlands, suggesting that coastal wetland vegetation plays a major role in decreasing current velocity, wave height, erosion of salt marshes over time, and sediment transport (Mendez and Losada 1999; Deng et al. 2010; Feagin et al. 2010; Coulombier et al. 2012; Torres et al. 2015; Vuik et al. 2016). Additionally, numerical modeling studies specifically focusing on water level analysis have also demonstrated the potential of vegetation to effectively attenuate storm surges in coastal areas

*Correspondence: jgarzon3@gmu.edu

(Järvelä 2005; Loder et al. 2009; Wamsley et al. 2010; Kourgialas and Karatzas 2013; Guannel et al. 2015; Haddad et al. 2016). Using numerical models, Wamsley et al. (2010) demonstrated the impact of wetland losses on coastal flooding and determined that the loss of wetlands could potentially increase water levels, suggesting that wetlands are an integral part of protecting the coastal infrastructure. However, they also pointed out that this protection is highly dependent on landscape characteristics and storm meteorological conditions. In another modeling study, Hu et al. (2015) used a Delft3D model simulation incorporating the vegetation effects on current flow and turbulence in a Louisiana wetland during storm surge events. They determined that as stem height, density, and diameter increases, attenuation directly increases.

Nevertheless, fewer studies based on field observations of water levels exist and of those attenuation analyses performed using field-collected data, mostly involve data from only one or a few storm surge events (Stark et al. 2015). A comprehensive list of studies investigating water level attenuation in coastal wetlands is presented in Table 1. For instance, USACE (USACE 1963) computed attenuation rates varying between 1.7 cm/km and 20 cm/km over distances up to 51 km of marshlands in Louisiana. Other studies also documented storm surge attenuation rates in the Gulf of Mexico region for two major hurricanes, Hurricane Andrew (1992) and Hurricane Rita (2005), and reported attenuation rates of 4.4–4.9 cm/km and 4–25 cm/km, respectively (Lovelace 1994; McGee et al. 2006).

The wide range of the storm surge attenuation rates documented in Table 1 supports Resio and Westerink's (2008) theory that the potential of wetlands to attenuate storm surge is highly dependent on several processes such as meteorological conditions, local bathymetry, surface roughness provided by the vegetation, and the presence of streams and other local characteristics. Wamsley et al. (2010) further demonstrated that while the wetlands do play a role in coastal protection, their effectiveness (e.g., attenuation rates) is variable along the coast due to landscape characteristics and dependent on storm parameters (mostly strength and duration), which explains the wide range of attenuation rates available in the literature. In this study, we further investigate the capacity of marshes to attenuate storm surge water level based on field measurements that resulted in a large collection (47 and 125 semidiurnal tidal cycles from up to 52 coastal flooding events) of attenuation rates for a wide range of storm conditions in two cross sections located in marshes of the Delmarva Peninsula (U.S. mid-Atlantic region). This large collection also provides a unique opportunity to broaden our understanding of the expected variation of attenuation rates in the same geographical location and within major storms. We expect that this study will contribute to the understanding of flood protection benefits associated with natural and nature-based features, and inform future coastal resilience efforts.

Methods

Study area

This study is based on water level monitoring campaigns at two natural reserve sites located in the U.S. mid-Atlantic region at the southern tip of the Delmarva Peninsula: the Eastern Shore of Virginia National Wildlife Refuge (hereafter ES) managed by the U.S. Fish and Wildlife Service and the Magothy Bay Natural Area Preserve (hereafter MGB) managed by the Virginia Department of Conservation and Recreation. The Delmarva Peninsula is a narrowing peninsula bordered by the Atlantic Ocean on the East Coast of the U.S. and the Chesapeake Bay (Fig. 1). The proximity of the study sites to the mouth of the Chesapeake Bay and the Atlantic Ocean result in a complex interaction of both water bodies and their hydrodynamic regime. The mean tidal amplitude is 0.9 m at the mouth of the bay. This amplitude increases from south to north through the Delmarva Peninsula. The average tidal current amplitude reported at the mouth is approximately 1 m/s (Xiong and Berger 2010) and was observed to be in phase with the water levels in the study area. Paquier et al. (2016) analyzed wind direction and speed in 2015 at the Chesapeake Bay Bridge Tunnel (CBBT) station (Fig. 1b) and observed that North winds (WNW to NE) and South-South-West winds (S to SW) are the most prevalent. Zhong and Li (2006) demonstrated that both tidal and wind forcing appear to have nearly equal importance in the hydrodynamics of the Chesapeake Bay.

The ES site is located just north of Fisherman Island National Wildlife Refuge, on the Atlantic Coast near the mouth of the Chesapeake Bay, behind an inlet created by the barrier island system that runs along most of the Delmarva Peninsula. This area is thus exposed to high currents during flood and ebb tides flowing in and out of the Chesapeake Bay, as well as high energy waves coming from the open Atlantic Ocean. The morphology of the area is characterized by a steep front edge and a relatively flat marsh platform (Fig. 2). This marsh is separated into two main parts: the lower marsh and the upper marsh. The lower marsh has low elevations (around 0–0.1 m above NAVD88) and is cut by a roughly 0.5 m deep and 5 m wide stream diverting into two shallow tributaries (Fig. 3). The upper marsh has a steeper slope (0.15%) and is inundated only during particularly high energy events. The marsh is bordered by an elevated forest (around 1.5 m), and the observed vegetation follows the same patterns found in other areas of the Chesapeake Bay region's coastal marshes (Knutson et al. 1982; Perry et al. 2001). The dominant species of vegetation is *Spartina alterniflora* in the lower marsh (Fig. 4) and *Spartina patens* in the upper marsh. *Distichlis spicata* and *Phragmites*

Table 1. Observed attenuation rates and maximum water levels in previous studies.

#	Authors	Data source	Surge type	Wetland type	Location	Attenuation (cm/km)	Max. water level (m)	Marsh area (km)
1	Lovelace (1994) in Wamsley et al. (2010)	Field	Hurricane Andrew, 1992	Marsh/open	Louisiana, U.S.A.	5.0	2.8 (MSL)	37.0
2	Lovelace (1994) in Wamsley et al. (2010)	Field	Hurricane Andrew, 1992	Marsh	Louisiana, U.S.A.	4.3	1.5 (MSL)	
3	Krauss et al. (2009)	Field	Hurricane Wilma, 2005	Marsh/mangrove	Florida, U.S.A.	4.0–6.9	1.0 (Above high tide conditions)	14.0
4	McGee et al. (2006), Wamsley et al. (2010)	Field	Hurricane Rita, 2005	Marsh	Louisiana, U.S.A.	10.0	4.1 (NAVD88)	3.2
5	McGee et al. (2006), Wamsley et al. (2010)	Field	Hurricane Rita, 2005	Marsh	Louisiana, U.S.A.	25.0	3.3 (NAVD88)	4.4
6	McGee et al. (2006), Wamsley et al. (2010)	Field	Hurricane Rita, 2005	Marsh	Louisiana, U.S.A.	4.0	3.4 (NAVD88)	4.6
7	McGee et al. (2006), Wamsley et al. (2010)	Field	Hurricane Rita, 2005	Marsh	Louisiana, U.S.A.	7.7	3.3 (NAVD88)	8.5
8	Resio and Westerink (2008)	Modeled	Hurricane Rita, 2005	N/A	Western Louisiana, U.S.A.	5.3–9.0	5	-
9	Resio and Westerink (2008)	Modeled	Hurricane Rita, 2005	N/A	Eastern Louisana, U.S.A.	−2.2	3	-
10	In Stark et al. (2015) calculated from figures in Van der Molen (1997)	Field	Tides	Tidal flat/marsh channel	Massachusetts, U.S.A.	−2.0 to 11	-	-
11	Army Corp of Engineers 1963	Field	Storm surge	Marsh	Louisiana, U.S.A.	6.9	4.5 (MSL)	51.0
12	Stark et al. (2015)	Field	Tides and storm surge	Marsh	Netherlands	−5.0 to 70.0	1.6 (∼MSL)	0.05–0.1
13	Krauss et al. (2009)	Field	Hurricane Charley, 2004	Marsh/ mangrove	Florida, U.S.A.	9.4–15.8	0.8 (Above high tide conditions)	5.5

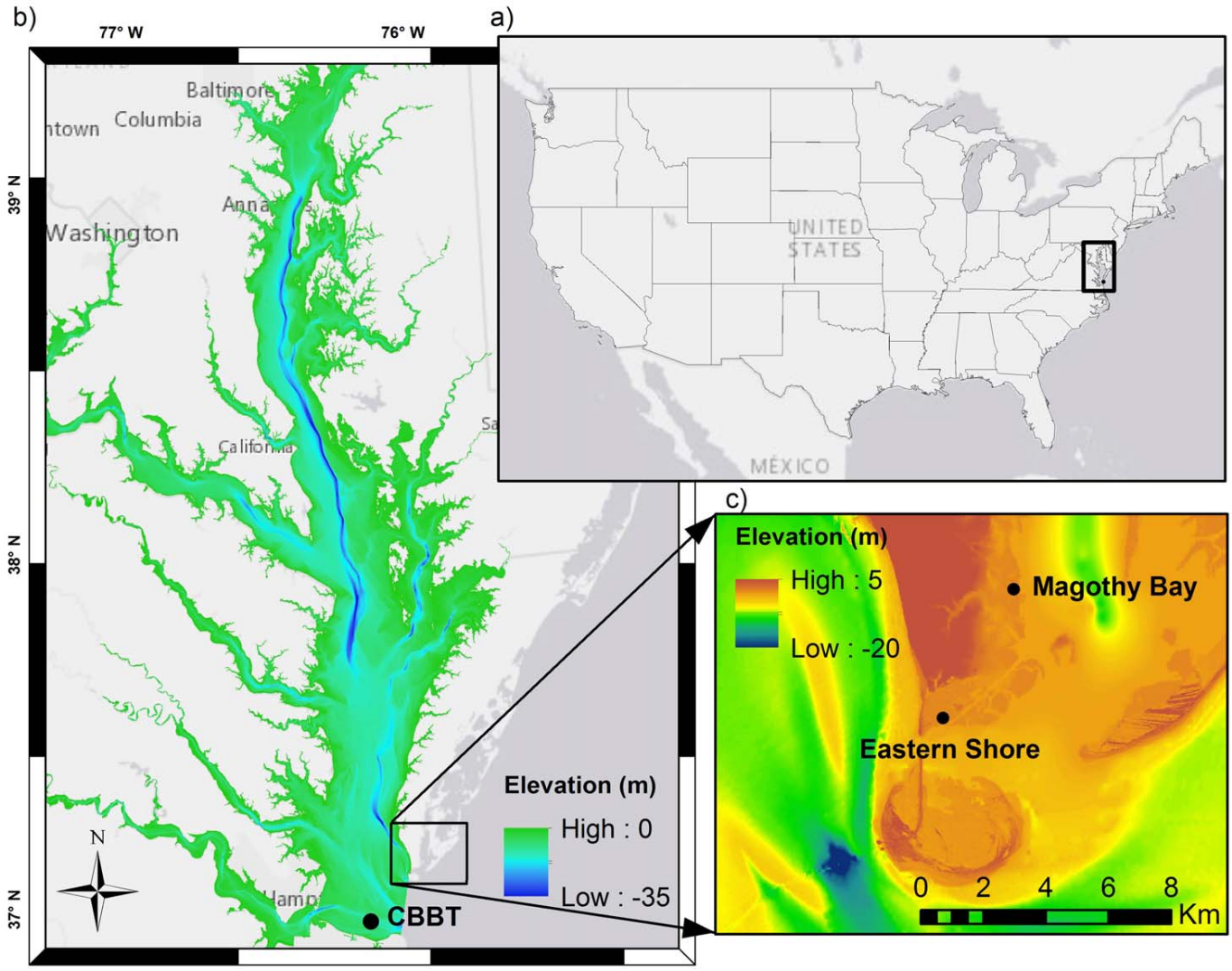

Fig. 1. (**a**) Location of Chesapeake Bay in the U.S. (**b**) Southeastern part of Delmarva Peninsula and the location of the NOAA monitoring station (CBBT). (**c**) Location of the two study sites, Eastern Shore and Magothy Bay. [Color figure can be viewed at wileyonlinelibrary.com]

australis are also present in the highest locations, bordering the forested areas.

The MGB site is located 5 km north of the ES site on the Eastern shore of the Delmarva Peninsula, behind the barrier islands. This marsh is similarly characterized by a steep and high front edge (around 0.2–0.3 m above NAVD88) and several representative channels within the marsh areas. The most significant channel, observed in Fig. 4, crosses the marsh platform almost perpendicular to the coast and reaches a levee (NAVD88 + 1.7 m) delimiting the marsh; its depths in this region vary between NAVD88 − 0.5 m and NAVD88 − 0.9 m. A smaller channel is present which diverges from the main channel, creating an alternate flow path toward the south. This channel is observed in Fig. 3 at 230 m from the origin of the profile. The elevation of the marsh platform varies from 0.2 m to 0.4 m in the lower marsh (before the diverging channel) and from 0.2 m to 0.7 m at the foot of the levee in the upper marsh (after the diverging channel). Some areas of the upper marsh present a lower elevation than the lower marsh, as shown in Fig. 3. Behind the levee, there is an artificial retention basin connecting this area to the marsh platform through a bypass. However, it was observed that all water flowing upstream through the main channel does not pass across the bypass, and a significant quantity of the flow accumulates at the shore side of the levee in the upper marsh platform. The same forest bordering ES extends in the back of the MGB marsh. The dominant vegetation species in this site is *Spartina alterniflora*.

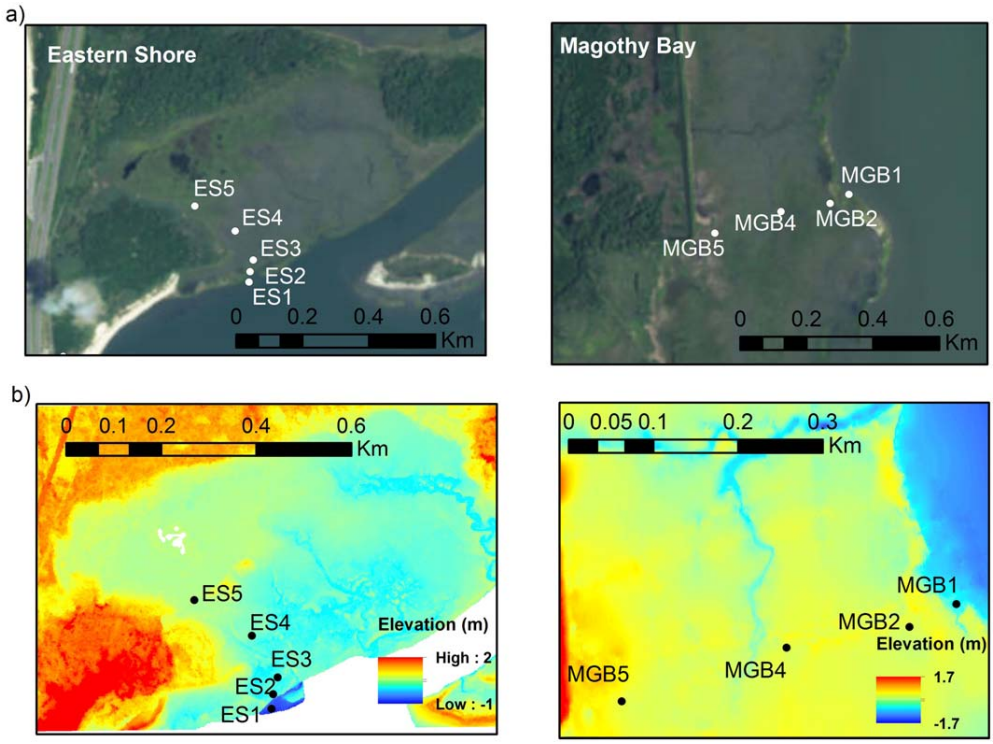

Fig. 2. (**a**) Aerial image of the study site indicating the position of the monitoring stations. (**b**) Digital elevation map. Left panel represents ES, and right panel displays MGB. [Color figure can be viewed at wileyonlinelibrary.com]

Paquier et al. (2016) conducted a vegetation survey at the ES site during the fall of 2015 (*see* Table 2) and observed that vegetation stem densities varied between 270 and 425 stem per m^2 at the lower marsh, but 760–870 stem per m^2 were found at the upper marsh. Plant heights showed a large variability. The tallest stems were observed close to the shoreline (more than 80 cm), generally decreasing at the backside of the marsh from 20 cm to 40 cm. Stem diameters were also larger at the lower marsh (5 mm) than those observed at the upper marsh (1–3 mm).

Additional vegetation surveys were conducted in August 2016 at the ES site, showing higher plant heights close to the shoreline (60–80 cm), and shorter plants at the upper marsh (40–50 cm). However, this survey revealed a lower stem density at the upper marsh than at the lower marsh. The stem diameters ranged from 4 mm to 8 mm. During March 2017, another vegetation survey was conducted at the MGB site. During spring, for *S. virginica* (located near the edge of the marsh and at the vicinity of the levee) the stem densities reported ranged from 2100 to 2400 stems per m^2, and the plant height was 10 cm. *S. alterniflora* distributed through the marsh platform exhibited a lower stem density, ranging from 200 stem per m^2 at the lower marsh and 600 stem per m^2 at the upper marsh. The height plant varied from 35 cm and 40 cm, respectively, and diameters of 1–3 mm were observed.

Water levels data collection

Water-level measurements were collected during two different time periods: the water levels at ES were monitored beginning in fall 2013 until the end of 2016; while the water-level measurements were taken at MGB during a shorter period, beginning in summer 2015 until the end of 2016 (Fig. 5a). The measurements were performed using a low frequency pressure transducer (Hobo onset U20L-01, U20-001-01 Ti and U20-001-04). Five monitoring stations were maintained at the ES site, while four monitoring stations were maintained at MGB. At each monitoring station, one pressure transducer was continually recording pressure measurements every 6 min. The sensor at each monitoring station was exchanged at approximately 3-month intervals for data collection and station maintenance. Additionally, one sensor was maintained in each study site to record the atmospheric pressure. The water levels were calculated with the ONSET proprietary Hoboware™ software based on the relative pressure difference measured at monitoring stations and the atmospheric pressure captured at each site. It is important to highlight that sensors measure the total pressure of the water column above the transducer, and therefore the water levels (free sea surface) calculated is a combination of the mean sea level and any other effects such as wave shoaling or wave breaking.

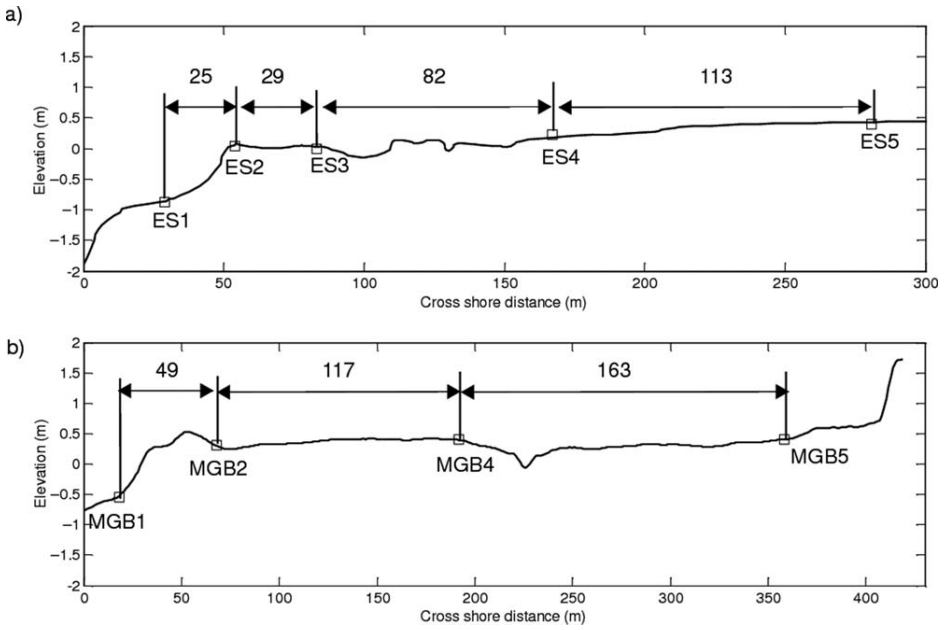

Fig. 3. Topo-bathymetric profile of the analyzed transects. Upper panel (a) represents the Eastern Shore (ES) site, stations (1–5), and lower panel (b) displays the Magothy Bay (MGB) site, stations (1–5). Units in the figure are given in meters (m).

Fig. 4. ES marsh edge (left), and aerial image of the marsh platform at MGB (right). [Color figure can be viewed at wileyonlinelibrary.com]

The monitoring stations were georeferenced and the elevations of the sensors at each station were measured with a differential GPS Trimble R4. The measured points were corrected by using the base antenna location through the Online Positioning User Service (http://www.ngs.noaa.gov/OPUS). For instance, the observed water levels at ES1 on 01 October 2015 shown in Fig. 6 were 1.08 m and −0.02 m respectively; meanwhile the water levels corresponding to the pictures are 1.33 m and 0.61 m at MGB. The configuration of the monitoring stations consists of five sensors along a 252 m transect at the ES site and four sensors along a 340 m transect at the MGB site (Fig. 3).

As displayed in Fig. 3a, at the ES site, sensor 1 (ES1) is located on the ocean side of the marsh at NAVD88-0.9 m. Sensor 2 (ES2) is on the edge of the marsh with an elevation of around NAVD88 + 0 m, and a distance of 24 m from sensor 1. Sensor 3 (ES3) is located at the lower marsh, before the tributaries and located 29 m from ES2. Sensor 4 (ES4) is located behind those tributaries at the upper marsh, and its elevation is NAVD88 + 0.2 m. The distance from the previous sensor is 84 m. Sensor 5 (ES5) is located on the backside of the marsh, with an elevation of NAVD88 + 0.4 m and 114 m to ES4.

The transect at MGB is shown in Fig. 3b. Sensor 1 (MGB1) is found on the seaside of the marsh edge at an elevation of NAVD88-0.5 m. Sensor 2 (MGB2) is located over the marsh platform 50 m from MGB1, with an elevation of NAVD88 + 0.3 m. Sensor 4 (MGB4), located seaward of the channel, has an elevation of NAVD88 + 0.4 m and is situated 120 m from the previous

Table 2. Vegetation properties.

	Stem density (n/m^2)	Diameter (mm)	Stem height (cm)
ES Fall 2015			
Lower marsh	270–425	4–7	50–90
Upper marsh	760–870	1–3	20–40
ES Summer 2016			
Lower marsh	350–500	4–8	60–90
Upper marsh	250	4–8	40–50
MGB Spring 2016			
Lower marsh	200–2100	1–3	11–40
Upper marsh	600–2400	1–3	10–35

sensor MGB2. Note that sensor 3 (MGB 3) was excluded from the analysis due to malfunctions. Sensor 5 (MGB5) is the farthest inland sensor with an elevation of NAVD88 + 0.4 m, and its distance from the previous sensor and the levee is 170 m and 50 m, respectively.

Data processing

The elevations of the sensors were used to evaluate and compute the water levels above NAVD88 at each monitoring station. The entire record of water levels is illustrated in Fig. 5a, including the gaps in recording due to sensor failures. The flood events were limited to time periods where all sensors along the transects were under water (note that ES5 and MGB5 were permanently dry during normal and high astronomical tidal conditions). By a comparison of the water level predictions and observations at the Chesapeake Bay Bridge Tunnel (CBBT) station, it was observed that storm surge ranged from 0.2 m to 1.06 m at ES and from 0.1 m to 1.06 m at MGB during the selected flood events. These events were further classified into five categories following the Advanced Hydrologic Prediction Service (AHPS) of National Weather Service (NWS) thresholds for the CBBT station (http://water.weather.gov/ahps2/hydrograph.php?wfo=akq&gage=cbbv2): (1) Major WL > 1.47 m, Moderate WL > 1.32 m, Minor WL > 1.17 m, Action WL > 1.02 m, Nominal WL < 1.02 m (Fig. 5a). Therefore, every tidal cycle during each specific flood event was analyzed, except for those events categorized as nominal. For the nominal events, the tidal cycle with the highest water levels was evaluated.

The water levels during high tides exhibit a significant scatter, especially the water levels recorded at the stations located closer to the coastline, which were exposed to wave effects (Fig. 5b). Therefore, the water level variations due to wave action at those stations directly impacted the calculation of attenuation rates, increasing or reducing the instantaneous water levels via passing of a wave crest or trough as well as the result of wave breaking. In order to reduce this variation, an 84 min (14 measurements) moving average calculation was performed. A sensitivity analysis was performed to evaluate the impact of the interval length on the resulting attenuation rates, and no changes in attenuation rates were observed for values larger than 84 min.

Attenuation rates along transects were computed as the reduction in peak water levels, obtained after the moving average calculation, between the sensor 1 (S1) and the sensor 5 (S5). Examples are depicted in Fig. 5c. Traditionally, centimeter per kilometer (cm/km) is used as attenuation rate units, even in studies considering inland distances of a few dozens of meters (Stark et al. 2015). However, centimeter per meter (cm/m) is used in this study since upscaling the attenuation rates to centimeter per kilometer over such short distances (i.e., hundreds of meters) might mislead the reader to neglect other processes affecting the flood propagation on larger scales, leading to an overestimation of the attenuation capacity of these ecosystems. Furthermore, in an attempt to isolate the effect of the specific features of each reach along transects, water level attenuation was also calculated between sensor 2 and sensor 5, sensor 2 and sensor 4, as well as between each consecutive sensors.

In total, 21 and 52 flood events, including 48 and 125 semidiurnal tidal cycles, were identified at the ES and MGB sites respectively. The larger number of flood events recorded at MGB could be explained by two reasons: (1) A larger tidal amplitude at this site and (2) a larger distance from the sea bottom to the transducer of the sensor observed on ES5 against MGB5 (around 12 cm).

For this study, we considered two sources of uncertainties: water level collection and vertical datum referencing. The error associated with the water level recording devices (HOBO onset) is provided by the manufacturer. For instance, the typical error of the Hobo Onset U20-001-01 Ti (mostly used during the different deployments) is defined as the 0.05% of the operation range (30 ft), and it is equal to 0.45 cm. Also, the accuracy of the DGPS obtained after processing the data was lower than 1.5 cm.

Additionally, we estimated the uncertainties related to the wave induced water level variability by calculating the moving standard deviation of the raw data (14 points or 84 min). The moving standard deviation at the moment of the peak water level was selected for each tidal cycle and each sensor. Figure 7 shows the overall average of the moving standard deviation of the water levels per site and sensor. The overall average standard deviation estimated at the ES site is significantly higher than the one estimated at the MGB site, most prominently at sensor 1 and 2. This may be due to the higher wave energy reaching the shoreline at ES, and therefore, a higher instantaneous effect of waves in the measurements. Furthermore, both sites behave similarly in terms of reduction of the mean standard deviation toward the inland sensors; the standard deviation is substantially higher in sensor 1 than sensor 5, located further inland from the shoreline and not significantly impacted by the wind waves. However, as Fig. 5c displays, a high variability is still observed, mainly on S1. This variability could be associated with the strong winds blowing offshore and rougher sea state conditions offshore during the storms.

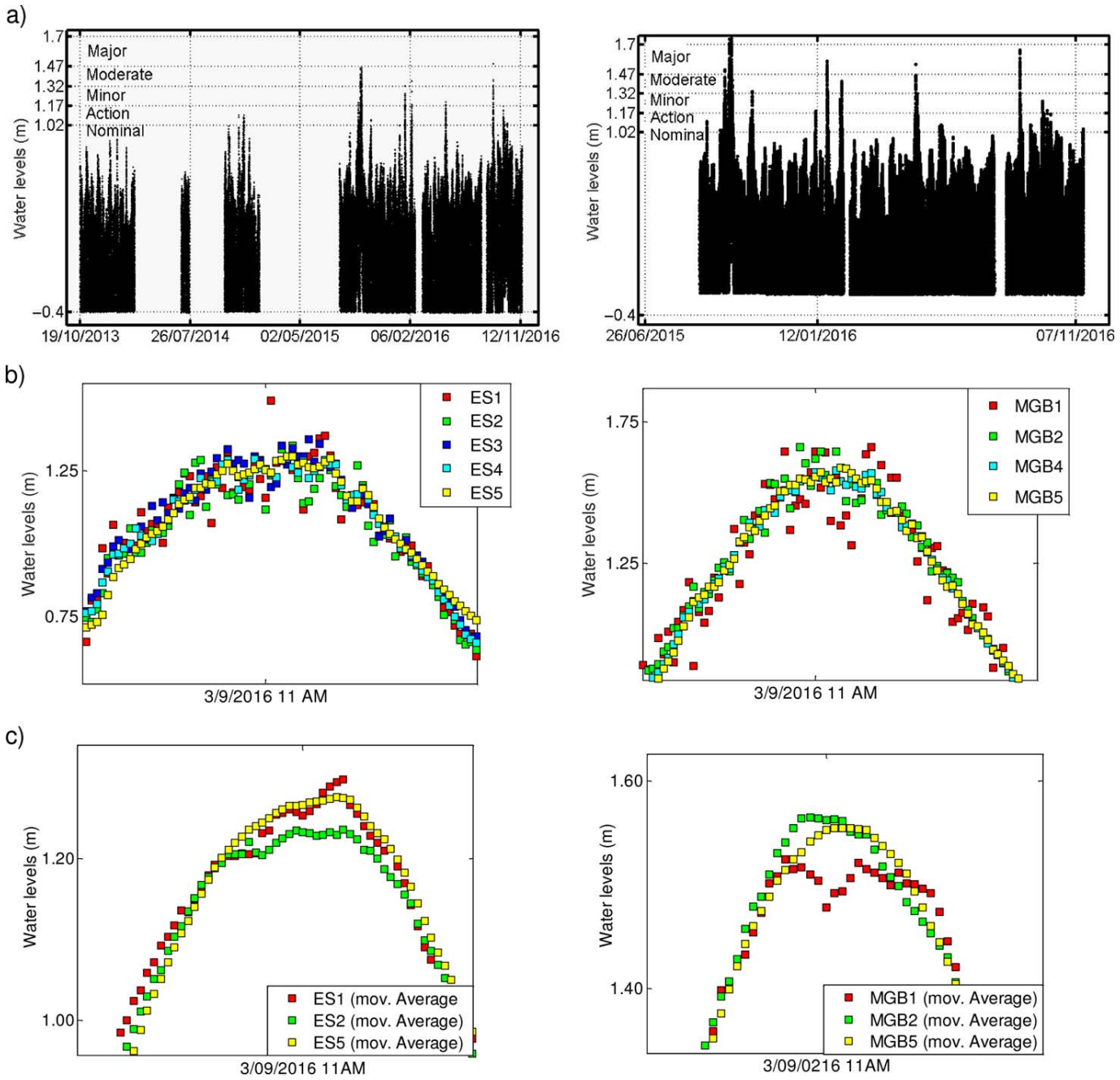

Fig. 5. (**a**) Complete dataset of water elevation above NADV88 at station 1. (**b**) Example of observed water elevation at each station during a given tidal cycle. (**c**) Moving average (84 min) water elevation at sensor 1, 2, and 5. Left side plots refer to ES and right side plots represent MGB. [Color figure can be viewed at wileyonlinelibrary.com]

Results and discussion

Overall attenuation rates

The attenuation rates calculated between ES1–ES5 and MGB1–MGB5 are plotted against the maximum water level at ES1 and MGB1 (seaside sensors) respectively and classified into the five storm categories (upper plots in Fig. 8). *Nominal* events at the ES site exhibited the largest attenuation rate variability, ranging from −0.01 cm/m to 0.02 cm/m, although water level amplification (negative attenuation) was only found during two events. The number of events classified as *action* events were significantly lower, and they mostly revealed a positive attenuation up to 0.02 cm/m.

Fig. 6. (**a**) Images of the marsh platform dry and (**b**) inundated. These images were taken during a severe event on 1st and 2nd of October 2015. Left plots correspond to ES and right plots correspond to MGB. [Color figure can be viewed at wileyonlinelibrary.com]

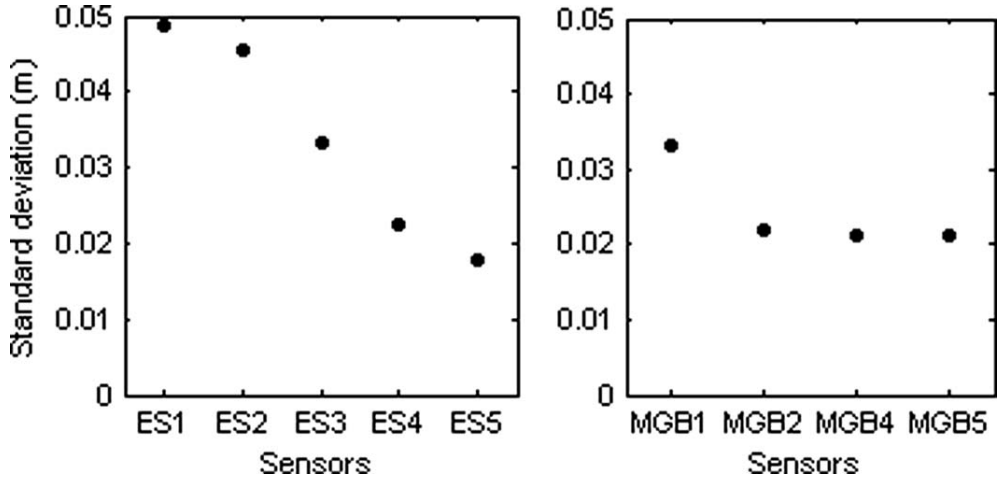

Fig. 7. The standard deviation averaged by using each tidal cycle per sensor and study site. Left plot corresponds to ES and right plot corresponds to MGB.

Three events categorized as *minor* events were recorded at ES, and their attenuation rates ranged from 0 cm/m to 0.010 cm/m. Finally, the attenuation rates of the two *moderate* events measured at ES varied from 0 cm/m to 0.01 cm/m. On the other hand, at MGB, most of the *nominal* events attenuation rates ranged between 0 cm/m and 0.02 cm/m. *Action* events mainly varied between 0 cm/m and 0.02 cm/m as well. Twelve *minor* events were observed at MGB, and most of the attenuation rates

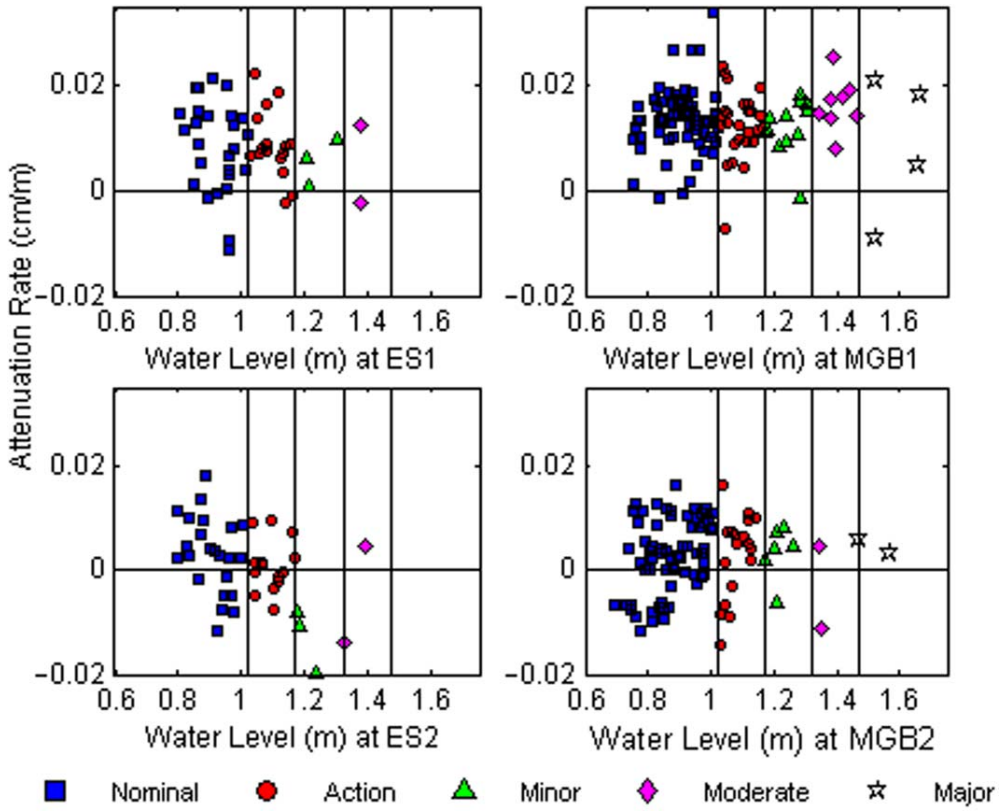

Fig. 8. Upper plots represent the attenuation rates (cm/m) between S1 and S5 (overall) vs. water level at S1. ES and MGB are represented in the left and right plot respectively. Lower plots represent the attenuation rate between S2 and S5 (marsh platform) vs. water level at S2. Positive and negative values represent water level attenuation and amplification respectively. The analyzed events were classified into the five categories presented previously. [Color figure can be viewed at wileyonlinelibrary.com]

ranged between 0.01 cm/m and 0.02 cm/m. The eight *moderate* events found at MGB exhibited values from 0.01 cm/m and 0.025 cm/m. Finally, four *major* events were recorded and their attenuation rates exhibited a large variability, showing values from −0.01 cm/m and 0.02 cm/m.

The attenuation rates of the nominal events varied from −0.01 cm/m to 0.02 cm/m at ES and 0 cm/m to 0.035 cm/m at MGB. Similarly, moderate and major events revealed also a wide range of attenuation rates, especially at the MGB site. This wide variation was also observed by Stark et al. (2015) across their short non-channeled transects (50–100 m) on the marsh platform in the Netherlands. Other studies performed on the East Coast of the U.S. such as van der Molen (1997) found that the astronomical tide elevations were attenuated from −2 cm/km (amplification) to 11 cm/km over a larger tidal marsh (Item 10 in Table 1). These findings are in accordance with our findings for the *nominal* events at ES. However, the reader should be aware of the smaller scale of our study sites in relation to most of the other studies in Table 1, representing significantly different realities.

Lower plots in Fig. 8 show the measured attenuation rates in the marsh platform (ES2-ES5 and MGB2-MGB5) against water levels. At ES, the *nominal* events displayed a large variability, ranging from −0.01 m/cm to 0.02 m/cm, but positive attenuation rates prevailed over negative rates. The *action* events mainly revealed a minimum water level attenuation or even water level amplification. During the three *minor* events observed, the water levels were amplified at the marsh platform; they exhibited the largest negative attenuation rates, from −0.01 cm/m to −0.02 cm/m. The attenuation rates of the two *moderate* events were −0.015 cm/m and 0.005 cm/m. At MGB, the *nominal* events displayed a large variability, varying between −0.01 cm/m and 0.02 cm/m. Similarly, *action* events varied from −0.015 cm/m to 0.015 cm/m. The *minor* events mostly revealed water level attenuation lower than 0.01 cm/m. The attenuation rates observed on the two *moderate e*vents were 0.005 cm/m and −0.01 cm/m, respectively; meanwhile the *major* events had positive attenuation (up to 0.005 cm/m).

Water levels were consistently higher at S1 than S2, and therefore a clear reduction in the ability of attenuating water level of the marsh platform (S2–S5) is observed in comparison to the overall transect (S1–S5) at both sites, as displayed in Fig. 8. The water levels at S1 are considerably more amplified

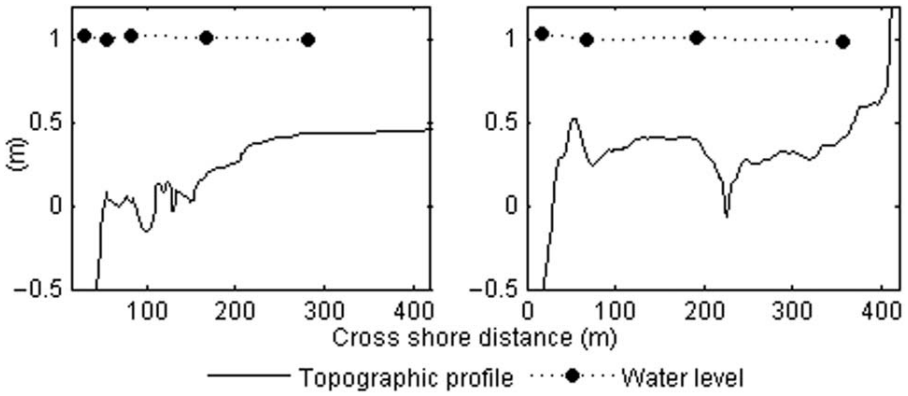

Fig. 9. Water level profiles across the marsh calculated by using the average attenuation rates between sensors and the average of the maximum water level at S1. Left plot corresponds to ES and right plot corresponds to MGB.

by wave setup than S2, as wave setup is positively correlated with the sea bottom slope, and moreover, the presence of vegetation between S1 and S2 reduces wave setup (van Rooijen et al. 2016). While it is noteworthy to mention that wave passing effects were mostly removed from the dataset, the edge of the marsh (and therefore the abrupt change in water depth) further filtered out the water level variability associated with strong wind or rougher sea states as noted on the dataset (*see* Fig. 5c). Therefore, the more exposed location of the S1 might affect the attenuation rate calculation and bias the results. Contrarily to the overall marsh, water levels within the marsh platform at ES exhibited a tendency of negative attenuation (water level amplification) with increasing water depth over the marsh. At the ES site, the marsh is surrounded by higher elevated forests, which produce a similar effect as a levee, impeding the movement of the wetting front. Hence, the water cannot propagate further inland, filling the storage area of the mash platform. The effect of a levee in water level attenuation has been discussed by previous authors, such as Resio and Westerink (2008). Based on numerical simulation results, they observed that the water levels increased across the marsh platform in Louisiana during Hurricane Rita (2005), reaching their maximum in front of the levee (Item 9 in Table 1). They also stated that this water level amplification would have been higher if the winds had been more intense. Also using numerical models, Stark et al. (2016) demonstrated that the presence of dikes could minimize the attenuation rates by a blockage effect. On the other hand, these implications have not been found at MGB. We hypothesize that the direction of the flow at this site is highly affected by the backside levee and incoming currents, which seems to orient the flow toward the N-S direction over the marsh platform (perpendicular to our water level measurements transect). This might have a direct impact on the attenuation rates measured by our cross-shore transect (E-W oriented). Additional studies with Acoustic Doppler Current Profiler (ADCP) or numerical models are necessary to further evaluate the impacts of the levee on the attenuation rates at this site.

Effects of landscape characteristics

To evaluate the effects of landscape characteristics within each marsh transect, attenuation rates between consecutive sensors were calculated to identify topographical features of the marsh platform that might play an important role in the attenuation of the water levels. Figure 9 depicts water level profiles across the marsh at each study site calculated by using the average attenuation rates between sensors and the average of the maximum water level at S1.

At ES, the average attenuation rate between ES1 and ES2 was 0.07 cm/m with the largest standard deviation (0.09 cm/m). The largest variability on attenuation rates found on the ES1–ES2 reach might be associated with the largest variation of water level at ES1 and to the short distance between sensors. Stark et al. (2015) also analyzed three short transects (50–100 m) located at the marsh platform and the marsh channel, and similarly, observed higher variability in the attenuation rates (the equivalent to a range from −0.005 cm/m to 0.07 cm/m). The higher attenuation capacity of this reach is also related to the impact of the edge (and therefore, abrupt change in water depth) and the contribution of wave set-up to each station. While ES1 is directly exposed to the tidal surge and wave setup, ES2 is located inland, and therefore, with relatively lower water depths and less exposed to wave set-up. Between ES2 and ES3, the average attenuation rate was negative (–0.08 cm/m), showing an amplification of the water levels between those sensors. ES2–ES3 also showed a large variability, but water levels mostly increased at S3. Likely, the lower elevation of S3 in comparison to S2 and S4 and the presence of the marsh channel, as Loder et al. (2009) demonstrated, might favor water accumulation in that part of the marsh and therefore, drastically reducing the attenuation rates. Furthermore, as Svendsen (1984) demonstrated, the roller effect carries a

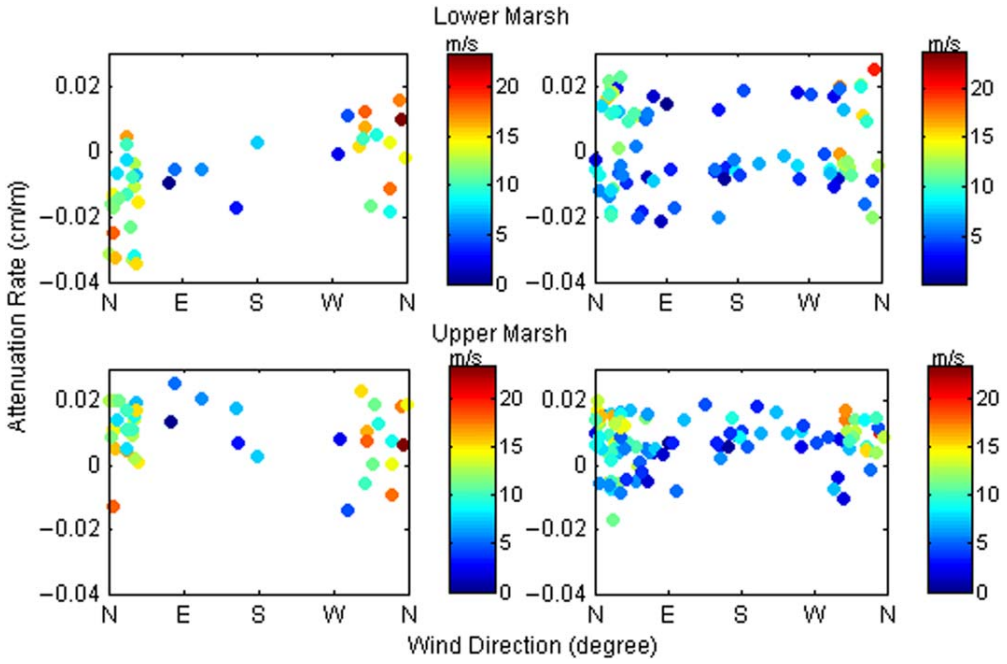

Fig. 10. Attenuation rates against wind direction at different sections of the marsh, lower marsh (S2–S4), and upper marsh (S4–S5). The color scale represents wind speed (m/s). Positive values depict water level attenuation. [Color figure can be viewed at wileyonlinelibrary.com]

significant volume of water shoreward. This highly turbulent region at the front of a breaker results in a substantial amount of radiation stress and energy flux. Therefore, after waves break over the edge, the roller effect transports mass of water inland, and then gradually decays further into the marsh platform. Between ES3 and ES4 the average attenuation rate was again positive, indicating a reduction of the water levels between those sensors. The average attenuation rate was 0.02 cm/m with a standard deviation of 0.02 cm/m, lower than the reaches closer to the edge of the marsh (ES1–ES2 and ES2–ES3). Finally, the lowest values of average attenuation rate and standard deviation were found at the backside reach. Between ES4 and ES5, the average attenuation and the standard deviation had values of 0.01 cm/m and 0.01 cm/m, respectively. Between these sensors, the bottom drag and flow resistance induced by the vegetation is more significant in the balance of the momentum forces than in the previous reaches where other processes were involved. The distance between ES3 and ES4, and ES4 and ES5 increased with respect to the previous reaches, and it might induce a lower variability in the rates as well. Furthermore, the blockage effect induced by the forest higher elevation at the end of the marsh might reduce the attenuation rates at this part of the marsh.

Similarly, at MGB, the highest average values and the standard deviation of those attenuation rates, 0.07 cm/m and 0.07 cm/m, respectively, were found between MGB1 and MGB2. The average attenuation rate between MGB2 and MGB4 was nearly zero, and the standard deviation had a significantly lower value (0.01 cm/m) than MGB1–MGB2. Similarly as simulated by Loder et al. (2009), the channel reduced the attenuation capacity of this reach. The average attenuation rates and standard deviations of the further inland reach, (MGB4–MGB5) were 0.01 cm/m and 0.01 cm/m, respectively, revealing the lowest value of standard deviation. However, as we hypothesized earlier, the location of the sensors, deployed on an E-W transect, might not properly capture the attenuation inside the marsh, and the levee might be inducing the flow circulation toward the N-S direction.

Wind effect on water level attenuation

Figure 10 explores the influence of the wind direction and speed on the attenuation rates at different portions of the marsh: lower marsh (S2–S4) and upper marsh (S4–S5). Wind characteristics were observed at the CBBT station during the peak of the storm surge at ES and MGB, respectively. The wind during the flood events at ES blew mainly from a range of 0 (North direction) ± 30°, and therefore, the angle between the transect and the wind direction ranged approximately from 0° to 45°. The number of events with winds blowing from other directions (East, West, or South) was limited, and they exhibited low wind speed (5–10 m/s). At MGB, the most severe storms were induced by winds coming from 0° ± 30°, which is perpendicular to the transect. Moreover, a significant number of flood events were reported with winds coming from other directions, although the wind speed was remarkably low. It is important to highlight

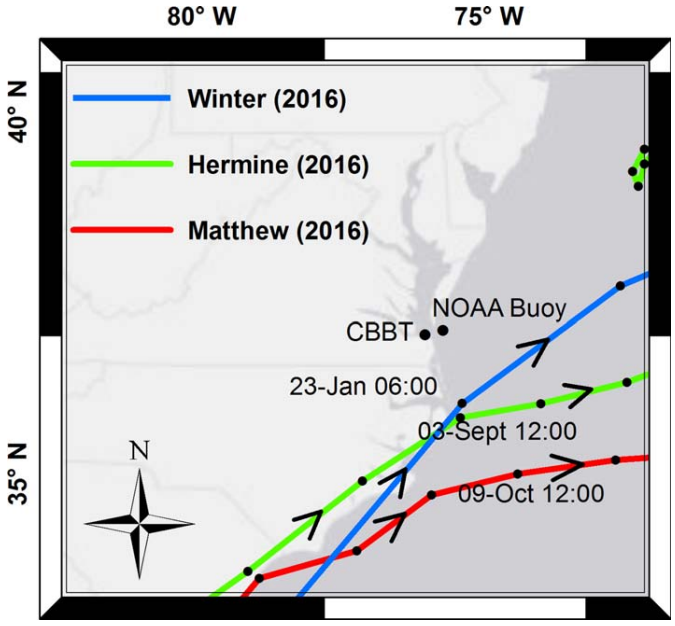

Fig. 11. Path of three major coastal events approaching the study area. CBBT is the meteorological station and NOAA buoy is the buoy where the wave heights were extracted. Dates represent the moment of the peak of the storm. [Color figure can be viewed at wileyonlinelibrary.com]

that the local wind direction does not necessarily represent the storm surge current direction, but the direction of the wind during the maximum water levels.

Our measurements did not display a clear relationship between wind characteristics and attenuation rates as suggested by Wamsley et al. (2010). For instance, at ES, during events with winds coming from NW, those rates ranged between −0.02 cm/m and 0.02 cm/m at both parts of the marsh platform. At both ES and MGB sites, the fetch of the wind over the marsh platform is very short, allowing minimal transfer of momentum from the wind to the water column, contrarily to other studies analyzing the wind influence on the water level attenuation. Furthermore, the surrounding forest vegetation has an impact on the upwind conditions from winds coming from N direction, reducing the wind-stress over the water column. Our study does not incorporate the impact of the storm forward speed on the attenuation rates, which can also have a significant impact on the resultant attenuation rates as suggested by Wamsley et al. (2010) and Resio and Westerink (2008), since the short distance between sensors limits this analysis. Other parameters, such as wind duration, might not have an important impact on the attenuation rates on these sites because the wind is acting over the water column only during certain hours in a semidiurnal tidal cycle, i.e., when the marsh is completely inundated. Thus, the extended time to transfer momentum from the wind to the water column over the marshes is very limited.

Attenuation rates variability within major storms

We further explored the attenuation of storm surge within the marshes for five severe events that were recorded during the monitoring period: September (2015) event, October (2015) event, Winter Storm (2016), Hurricane Hermine (2016), and Hurricane Matthew (2016). This analysis includes wind characteristics, wave heights, maximum water levels, astronomical tides, and surge. Winter Storm (2016) was a nor'easter system that emerged over the Atlantic Ocean at North Carolina and continued moving rapidly toward the northeastern over the open ocean as displayed in Fig. 11. Its winds blew from the NW varying between 18 m/s and 11 m/s (Table 3). This cyclone induced the highest waves and surge, although the astronomical high tide was significantly low (0.25 m). Hurricane Hermine (2016) emerged just to the south of the nor'easter event location, moving eastward later over the open ocean. The maximum wind speed reported on the study area reached up to 18 m/s. Hurricane Matthew (2016) moved parallel to the coast from Florida to North Carolina and it turned eastward moving over the open ocean. It induced the highest wind speed (N direction), but the center of the storm did not approach sufficiently to the study area to generate a significant surge. Furthermore, the astronomical high tide was low (0.3 m). On the other hand, September (2015) and October (2015) events (not shown in Fig. 11) were the most persistent events with north winds blowing between 7 m/s and 17 m/s and lasting for several days. These events were the combination of high tides (0.5–0.7 m) and onshore gale-force winds from a storm located at the mid-Atlantic Region coast.

Due to the intrinsic limitations of the MGB monitoring stations set-up, along with the fact that the wind direction observed during these events had mainly a north component, which is perpendicular to the orientation of the transect, this site was omitted from this analysis and further investigations were only conducted at the ES site. During the September (2015) event, the water levels were amplified at the lower marsh between −0.003 cm/m and −0.16 cm/m, meanwhile the water levels were attenuated at the upper marsh, except during the peak of the storm when the rate was 0.0 cm/m, as displayed in Table 3. Similarly, during the October (2015) event, the water levels were mainly amplified at the lower marsh, ranging from 0.004 cm/m to −0.03 cm/m, and attenuated at the upper marsh; at this part, the rates increased with lower high water levels (HWL) and exhibiting minimum rates during the two peaks of the storm. During Winter Storm (2016), the lower marsh induced water level attenuation (0.007 cm/m) and amplification (–0.011 cm/m and −0.016 cm/m). At the upper marsh, the water levels were amplified during the peak of the storm (–0.009 cm/m) and attenuated with lower water levels. During the Hurricane Hermine (2016) event, the lower marsh mainly amplified water levels up to −0.023 cm/m as well. However at the upper marsh, the largest attenuation (0.014 cm/m) was observed

Table 3. Environmental conditions observed during the five major coastal events: date, wind direction (degrees), wind speed (m/s), significant wave height (m), high water level at S1 (m), astronomical high tide (m) and surge(m), and lower and upper represent the attenuation rate (cm/m) at each section of the marsh.

Date	WDIR	WSPD	WVHT	HWL	AHT	SURGE	LOWER	UPPER
September (2015)								
26/09/2015 10:00	31	13	2.34	0.963	0.565	0.398	−0.011	0.014
26/09/2015 22:00	36	14.7	2.80	1.128	0.602	0.526	−0.157	0.000
27/09/2015 10:00	31	12.6	2.77	1.057	0.65	0.407	−0.003	0.022
27/09/2015 23:00	32	9.0	2.20	0.958	0.62	0.338	−0.032	0.153
28/09/2015 12:00	33	7.3	1.87	0.906	0.698	0.208	−0.007	0.194
October (2015)								
01/10/2015 14:00	1	12.5	2.14	1.066	0.689	0.377	−0.030	0.020
02/10/2015 02:00	359	14.3	2.98	1.113	0.46	0.653	−0.002	0.019
02/10/2015 14:00	8	15.8	3.17	1.378	0.619	0.759	−0.031	0.005
03/10/2015 02:00	6	14.3	3.02	1.138	0.403	0.735	−0.014	0.011
03/10/2015 15:00	29	10.2	2.31	1.159	0.571	0.588	−0.007	0.011
04/10/2015 03:00	33	15.4	3.10	1.204	0.343	0.861	−0.032	0.017
04/10/2015 15:00	23	16.8	3.44	1.379	0.51	0.869	0.004	0.004
05/10/2015 05:00	6	14.2	3.54	1.153	0.340	0.813	−0.013	0.011
05/10/2015 17:00	3	11.4	3.06	1.123	0.451	0.672	−0.016	0.008
Winter (2016)								
23/01/2016 08:00	341	17.9	4.16	1.210	0.255	0.955	−0.011	−0.009
23/01/2016 23:00	311	16.2	3.45	1.026	0.273	0.753	0.007	0.010
24/01/2016 11:00	318	11.1	3.02	1.015	0.447	0.568	−0.016	0.000
Hermine (2016)								
03/09/2016 12:00	5	18	3.42	1.298	0.503	0.795	−0.023	−0.013
03/09/2016 01:00	340	14.2	3.80	1.079	0.446	0.633	0.002	0.000
04/09/2016 14:00	340	8.9	2.42	0.972	0.496	0.476	−0.017	0.008
04/09/2016 03:00	11	7.9	2.23	0.864	0.415	0.449	−0.006	0.014
05/09/2016 15:00	324	9.2	2.26	0.870	0.438	0.432	0.005	0.013
Matthew (2016)								
09/10/2016 05:00	354	23.5	3.11	0.976	0.278	0.698	0.009	0.006
09/10/2016 17:00	311	18.2	3.40	0.859	0.381	0.478	0.011	0.007

with the lowest values of HWL, followed by a gradual reduction of the attenuation rates with higher water levels (up to 0 cm/m) and water level amplification during the peak of the storm (–0.01 cm/m). The lower marsh behaved differently during Hurricane Matthew (2016), which induced the lowest HWL, and water levels showed an attenuation of 0.01 cm/m. The upper part also attenuated the water levels (0.006 cm/m and 0.007 cm/m), with slightly lower rates during the peak of the storm.

Figure 12 shows that within each event, the capacity of the upper marsh to attenuate water level decreases with higher HWL. Additionally, water level amplification occurred at this section of marsh for certain events with water levels over 1.2 m depth at ES4 (Winter Storm [2016] and Hurricane Hermine [2016] events). Stark et al. (2015) observed that water levels were attenuated only during events that resulted in water levels between 0.5 m and 1 m above the marsh platform and minimum attenuation or amplification was found on the highest recorded storm tides. These observations are in concordance with our findings and the lowest rates or water level amplifications were computed during the highest storm tides. We also observed that these effects could be a result of an increase in the storage area, a reduced bottom friction for higher water depths and lower friction exerted over the flow by the vegetation submergence in accordance with Stark et al. (2015).

Figure 12 also displays that with similar HWL, the ability of attenuating water level varied per storm. For instance, inundation heights of 0.96 m were attenuated with a rate of 0.007 cm/m and 0.014 cm/m during Hurricane Hermine (2016) and September (2015) events respectively. As Resio and Westerink (2008) stated, attenuation rates depend on multiple factors including storm characteristics, local and regional topography and bathymetry and surface roughness or wind waves. Although the local and regional landscape and bathymetry are mainly stationary, further analyses comprising a combination

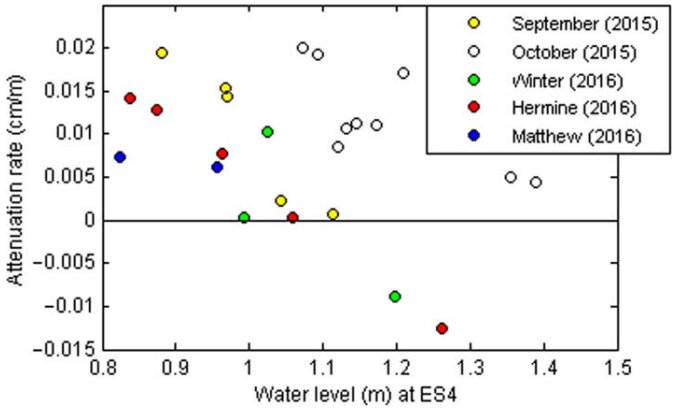

Fig. 12. Attenuation rates (cm/m) at the upper marsh against the maximum water levels observed at ES4 for the duration of five major coastal storms. Positive values depict water level attenuation. [Color figure can be viewed at wileyonlinelibrary.com]

of these factors might clarify the understanding of the inland flood propagation at ES. Additionally, we hypothesize that the current's direction and magnitude play a major role in the attenuation rates at the local scale and supplementary field studies are necessary to evaluate this variation further.

Conclusions

In order to improve our understanding of the ability of marshes to attenuate storm surge, we collected water level data in two natural preserve areas of the Delmarva Peninsula in the mid-Atlantic region of the U.S., the Eastern Shore of Virginia National Wildlife Refuge and the Magothy Bay Natural Area Preserve. In total, 47 and 125 semidiurnal tidal cycles respectively were measured under a wide range of storm conditions, resulting in the largest field-collected water level dataset found in the literature to date that is dedicated to studying storm surge attenuation by wetlands.

The overall marsh (marsh platform plus the marsh edge) attenuated water level with rates up to 0.02 cm/m at the Eastern Shore of Virginia National Wildlife Refuge (ES) and 0.03 cm/m at Magothy Bay Natural Preserve (MGB). The attenuation capacity of the ES site was drastically reduced if only the marsh platform was considered and even water level amplification was observed during several events. A closer analysis within the marsh sections also demonstrated that different parts of the marsh play different roles in the storm surge attenuation. The S1–S2 reach was the most effective section attenuating water level due to two reasons: the impact of the edge of the marsh and reduced wave setup propagation at the landside of the marsh. Our results also indicated a flow accumulation near the channels, a flux transportation carried by the roller effects near S3, and the lowest attenuation rates in the upper marsh.

Further analyses were conducted on the upper marsh at ES within five major events (September [2015], October [2015], Winter Storm [2016], Hurricane Hermine [2016], and Hurricane Matthew [2016]), revealing a reduction of the attenuation capacity with higher HWL. Furthermore, attenuation rates were significantly low or even negative (amplification) during the peak of the storms. This reduced attenuation or water level amplification might be the result of limitations in the storage area and lower bottom and vegetation friction induced by higher inundation heights. Nevertheless, the ability of the upper marsh to attenuate storm surge water level varied for each storm. Thus, the attenuation rates during the peaks of these five events ranged from −0.013 cm/m to 0.006 cm/m. These results indicate that this type of marshland would increase the attenuation during low inundation heights, but these ecosystems would be less effective attenuating high water depths.

Our study sites present specific characteristics that directly impact the water level attenuation processes: (1) the more exposed location of S1, highly affected by rougher sea states, led to higher water levels and therefore an overestimation of the attenuation rates; (2) the short spatial scale (200–400 m) might imply that processes playing an important role on larger scales such as transfer of momentum from the wind to the water and dynamic interactions between flow and vegetation, were less significant at these sites; (3) the coastal circulation and the backside levee at MGB oriented the currents toward the N-S direction, and therefore, the sensors located at an E-W transect might not have properly captured the water level attenuation inside the marsh; and (4) the elevated forest surrounding ES increased the storage area on the marsh platform during high inundation heights.

Overall, we found that the greatest attenuation rates occurred at the marsh edge. The inland reach close to the coastline revealed an amplification of the water level followed by water level attenuation toward the inland areas. Additionally, small spatial scales of the marsh platform, geomorphological features such as channels, elevated surrounding forest and levees seem to play a major role in reducing the attenuation rates provided by marshes. These results indicate that, while this type of marshland would provide storm surge attenuation during low inundation heights, these ecosystems would be less effective at attenuating higher water depths from extreme events. Finally, for marshes with spatial scales on the order of 200–400 m, such as areas commonly found in the Chesapeake Bay and worldwide, an absolute storm surge attenuation lower than 5 cm might undervalue the importance of marshes in providing coastal protection. However, the storm surge reduction benefits should not be considered alone but in conjunction with the potential for wave and current attenuation, which are not evaluated in this study.

Future studies should also consider documenting the current direction and magnitude and its impact on attenuation

rates within the marsh areas to further explore its importance when quantifying the marshes protective capabilities. Additionally, high-resolution numerical models could provide further insights into the influence of local hydrodynamic process on the attenuation rates within the same storm, providing additional support for restoration and preservation design efforts.

References

Arkema, K. K., and others. 2013. Coastal habitats shield people and property from sea-level rise and storms. Nat. Clim. Chang. **3**: 913–918. doi:10.1038/nclimate1944

Barbier, E. B., I. Y. Georgiou, B. Enchelmeyer, and D. J. Reed. 2013. The value of wetlands in protecting southeast Louisiana from hurricane storm surges. PLoS One **8**: 1–6. doi:10.1371/journal.pone.0058715

Committee on Environment and Resources, National Science and Technology Council. 2015. Ecosystem-Service Assessment: Research Needs for Coastal Green Infrastructure. Executive Office of the President of the United States.

Coulombier, T., U. Neumeier, and P. Bernatchez. 2012. Sediment transport in a cold climate salt marsh (St. Lawrence Estuary, Canada), the importance of vegetation and waves. Estuar. Coast. Shelf Sci. **101**: 64–75. doi:10.1016/j.ecss.2012.02.014

Cui, W., and L. Caracoglia. 2016. Exploring hurricane wind speed along US Atlantic coast in warming climate and effects on predictions of structural damage and intervention costs. Eng. Struct. **122**: 209–225. doi:10.1016/j.engstruct.2016.05.003

Deng, Y., H. M. Solo-Gabriele, M. Laas, L. Leonard, D. L. Childers, G. He, and V. Engel. 2010. Impacts of hurricanes on surface water flow within a wetland. J. Hydrol. **392**: 164–173. doi:10.1016/j.jhydrol.2010.08.004

Feagin, R. A., and others. 2010. Shelter from the storm? Use and misuse of coastal vegetation bioshields for managing natural disasters. Conserv. Lett. **3**: 1–11. doi:10.1111/j.1755-263X.2009.00087.x

Guannel, G., P. Ruggiero, J. Faries, K. Arkema, M. Pinsky, G. Gelfenbaum, A. Guerry, and C. K. Kim. 2015. Integrated modeling framework to quantify the coastal protection services supplied by vegetation. J. Geophys. Res. C **120**: 324–345. doi:10.1002/2014JC009821

Haddad, J., S. Lawler, and C. M. Ferreira. 2016. Assessing the relevance of wetlands for storm surge protection: A coupled hydrodynamic and geospatial framework. Nat. Hazards **80**: 839–861. doi:10.1007/s11069-015-2000-7

Hu, K., Q. Chen, and H. Wang. 2015. A numerical study of vegetation impact on reducing storm surge by wetlands in a semi-enclosed estuary. Coast. Eng. **95**: 66–76. doi:10.1016/j.coastaleng.2014.09.008

Järvelä, J. 2005. Effect of submerged flexible vegetation on flow structure and resistance. J. Hydrol. **307**: 233–241. doi:10.1016/j.jhydrol.2004.10.013

Knutson, P. L., R. A. Brochu, W. N. Seelig, and M. Inskeep. 1982. Wave damping in Spartina alterniflora marshes. Wetlands **2**: 87–104. doi:10.1007/BF03160548

Kourgialas, N. N., and G. P. Karatzas. 2013. A hydro-economic modelling framework for flood damage estimation and the role of riparian vegetation. Hydrol. Process. **27**: 515–531. doi:10.1002/hyp.9256

Krauss, K. W., T. W. Doyle, T. J. Doyle, C. M. Swarzenski, A. S. From, R. H. Day, and W. H. Conner. 2009. Water level observations in mangrove swamps during two hurricanes in Florida. Wetlands **29**: 142–149. doi:10.1672/07-232.1

Lavoie, R., J. Deslandes, and F. Proulx. 2016. Assessing the ecological value of wetlands using the MACBETH approach in Quebec City. J. Nat. Conserv. **30**: 67–75. doi:10.1016/j.jnc.2016.01.007

Loder, N. M., J. L. Irish, M. A. Cialone, and T. V. Wamsley. 2009. Sensitivity of hurricane surge to morphological parameters of coastal wetlands. Estuar. Coast. Shelf Sci. **84**: 625–636. doi:10.1016/j.ecss.2009.07.036

Lovelace, J. K. 1994. Storm-tide elevations produced by Hurricane Andrew along the Louisiana Coast, August 25–27, 1992. U.S. Geological. Survey.

McGee, B. D., B. B. Goree, T. R. W. K. Woodward, and W. H. Kress. 2006. Hurricane Rita Surge Data, Southwestern Louisiana and Southeastern Texas, September to November 2005. U.S. Geological Survey.

Mendez, F. J., and I. J. Losada. 1999. Hydrodynamics induced by wind waves in a vegetation field. J. Geophys. Res. **104**: 18383–18396.

Narayan, S., and others. 2016. The effectiveness, costs and coastal protection benefits of natural and nature-based defences. PLoS One **11**: 1–17. doi:10.1371/journal.pone.0154735

National Research Council of the National Academy of Sciences. 2014. Reducing Coastal Risks on the East and Gulf Coasts. (National Academy of Sciences), doi:10.17226/18811

Paquier, A.-E., J. Haddad, S. Lawler, and C. M. Ferreira. 2016. Quantification of the attenuation of storm surge components by a coastal wetland of the US Mid Atlantic. Estuaries Coast. **40**: 930–946. doi:10.1007/s12237-016-0190-1

Perry, J. E., T. A. Barnard, J. G. Bradshaw, C. T. Friedrichs, K. J. Havens, P. A. Mason, W. I. Priest, and G. M. Silberhorn. 2001. Creating tidal salt marshes in the Chesapeake Bay. J. Coast. Res. 170–191.

Resio, D. T., and J. J. Westerink. 2008. Modeling the physics of storm surges. Phys. Today **61**: 33–38. doi:10.1063/1.2982120

Stark, J., T. Van Oyen, P. Meire, and S. Temmerman. 2015. Observations of tidal and storm surge attenuation in a large tidal marsh. Limnol. Oceanogr. **60**: 1371–1381. doi:10.1002/lno.10104

Stark, J., Y. Plancke, S. Ides, P. Meire, and S. Temmerman. 2016. Coastal flood protection by a combined nature-based and engineering approach: Modeling the effects of marsh geometry and surrounding dikes. Estuar. Coast. Shelf Sci. **175**: 34–45. doi:10.1016/j.ecss.2016.03.027

Sutton-Grier, A. E., K. Wowk, and H. Bamford. 2015. Future of our coasts: The potential for natural and hybrid infrastructure to enhance the resilience of our coastal communities, economies and ecosystems. Environ. Sci. Policy **51**: 137–148. doi:10.1016/j.envsci.2015.04.006

Svendsen, I. A. 1984. Mass flux and undertow in a surf zone. Coast. Eng. **8**: 347–365. doi:10.1016/0378-3839(84)90030-9

Torres, J. M., B. Bass, N. Irza, Z. Fang, J. Proft, C. Dawson, M. Kiani, and P. Bedient. 2015. Characterizing the hydraulic interactions of hurricane storm surge and rainfall-runoff for the Houston-Galveston region. Coast. Eng. **106**: 7–19. doi:10.1016/j.coastaleng.2015.09.004

U.S. Army Corps of Engineers (USACE). 1963. Interim Survey Report, Morgan City, Louisiana and Vicinity, serial no. 63. U.S. Army Engineer District, New Orleans, LA.

van der Molen, J. 1997. Tidal distortion and spatial differences in surface flooding characteristics in a salt marsh: Implications for sea-level reconstruction. Estuar. Coast. Shelf Sci. **45**: 221–233. doi:10.1006/ecss.1997.0179

van Rooijen, A. A., R. T. McCall, J. S. M. van Thiel de Vries, A. R. van Dongeren, A. J. H. M. Reniers, and J. A. Roelvink. 2016. Modeling the effect of wave-vegetation interaction on wave setup. J. Geophys. Res. Oceans **121**: 4341–4359. doi:10.1002/2015JC011392

Vuik, V., S. N. Jonkman, B. W. Borsje, and T. Suzuki. 2016. Nature-based flood protection: The efficiency of vegetated foreshores for reducing wave loads on coastal dikes. Coast. Eng. **116**: 42–56. doi:10.1016/j.coastaleng.2016.06.001

Wamsley, T. V., M. A. Cialone, J. M. Smith, J. H. Atkinson, and J. D. Rosati. 2010. The potential of wetlands in reducing storm surge. Ocean Eng. **37**: 59–68. doi:10.1016/j.oceaneng.2009.07.018

Wobus, C., M. Lawson, R. Jones, J. Smith, and J. Martinich. 2013. Estimating monetary damages from flooding in the United States under a changing climate. J. Flood Risk Manag. **7**: 217–229. doi:10.1111/jfr3.12043

Xiong, Y., and C. R. Berger. 2010. Chesapeake Bay tidal characteristics. J. Water Resource Prot. **2**: 619–628. doi:10.4236/jwarp.2010.27071

Zhong, L., and M. Li. 2006. Tidal energy fluxes and dissipation in the Chesapeake Bay. Cont. Shelf Res. **26**: 752–770. doi:10.1016/j.csr.2006.02.006

Acknowledgments

This material is based upon work supported by the National Fish and Wildlife Foundation and the U.S. Department of the Interior under Grant 43932. The views and conclusions contained in this document are those of the authors and should not be interpreted as representing the opinions or policies of the U.S. Government or the National Fish and Wildlife Foundation and its funding sources. Mention of trade names or commercial products does not constitute their endorsement by the U.S. Government, or the National Fish and Wildlife Foundation or its funding sources. This material is also based upon work supported by the National Science Foundation under Grant SES-1331399. Any opinions, findings, and conclusions or recommendations expressed in this material are those of the authors and do not necessarily reflect the views of the National Science Foundation. This research was also supported in part by the Thomas F. and Kate Miller Jeffress Memorial Trust, Bank of America, Trustee. The authors would like to express their highest appreciations for former team members that collaborated with data collection over time; Beverly Lanza, Alayna Bigalbal, and Jana Haddad. Additionally, the authors really appreciate all the support from their partners at the DCR/VA and the USFWS that without their support, this work would not have been possible.

Conflict of Interest

None declared.

Submitted 15 March 2017
Revised 16 June 2017
Accepted 31 July 2017

Associate editor: Bernadette Sloyan